# Size-Dependent Tuning of $Mn^{2+}$ d Emission in $Mn^{2+}$-Doped CdS Nanocrystals: Bulk vs Surface

**Angshuman Nag,[†] Roby Cherian,[⊥,‡] Priya Mahadevan,[‡] Achanta Venu Gopal,[§] Abhijit Hazarika,[†] Akshatha Mohan,[§] A. S. Vengurlekar,[§] and D. D. Sarma*[,†]**

*Solid State and Structural Chemistry Unit, Indian Institute of Science, Bangalore-560 012, India, S. N. Bose National Centre for Basic Sciences, JD Block, Sector 3, Salt Lake, Kolkata 700098, India and, Department of Condensed Matter Physics and Material Sciences, Tata Institute of Fundamental Research, Homi Bhabha Road, Colaba, Mumbai 400 005, India*

*Received: June 21, 2010; Revised Manuscript Received: September 28, 2010*

We show that the characteristic $Mn^{2+}$ d emission color from $Mn^{2+}$-doped CdS nanocrystals can be tuned over as much as 40 nm, in contrast to what should be expected from such a nearly localized d−d transition. This is achieved surprisingly by a fine-tuning of the host particle diameter from 1.9 to 2.6 nm, thereby changing the overall emission color from red to yellow. Systematic experiments in conjunction with state-of-the-art ab initio calculations with full geometry optimization establish that $Mn^{2+}$ ions residing at surface/subsurface regions have a distorted tetrahedral coordination resulting in a larger ligand field splitting. Consequently, these near-surface $Mn^{2+}$ species exhibit a lower $Mn^{2+}$ d emission energy, compared to those residing at the core of the nanocrystal with an undisturbed tetrahedral coordination. The origin of the tunability of the observed $Mn^{2+}$ emission is the variation of emission contributions arising from $Mn^{2+}$ doped at the core, subsurface, and surface of the host. Our findings provide a unique and easy method to identify the location of an emitting $Mn^{2+}$ ion in the nanocrystal, which would be otherwise very difficult to decipher.

## Introduction

$Mn^{2+}$-doped semiconductor nanocrystals (NCs) exhibit strong dopant-related emissions at energies substantially lower than the host bandgap, overcoming the vexing problem of self-absorption,[1−8] in contrast to the excitonic emission[9−12] of their undoped counterpart. Also, the emission from doped NCs are relatively less sensitive to thermal and photochemical disturbances compared to those from the undoped samples.[5,13] On the basis of these advantages, doped semiconductor NCs have attracted increasingly more attention as superior phosphor materials for light emitting devices (LEDs)[4,14,15] and nontoxic biological labels.[16,17] Ironically, the basis for these substantial advantages is also the source of the most important disadvantage of such doped NCs as phosphor materials, namely one cannot tune the color of the dopant emission by tuning particle size, unlike the excitonic emission.

$Mn^{2+}$ 3d states are essentially localized, atomic-like states, with characteristic orbital spread much smaller than the typical NC size; thus, a change in the NC size has no perceptible effect on dopant $Mn^{2+}$ emission, leading to a near constancy of the emission energy at ∼2.12 eV (585 nm). One can achieve discrete emission colors, rather than a near-continuous tunability from doped semiconductor NCs by changing the transition metal dopant ion;[18] however, Xie et al.[19] achieved tunable emission color from Cu-doped InP NCs by tuning the energy of the bottom of the conduction band, which is one of the two energy states involved in the assigned dopant emission. Such a tuning of dopant emission is analogous to the bandgap tuning of the undoped host and is inherently different from the tuning of atomic-like $Mn^{2+}$ d−d transition. So far, there has been only one report[5] of tuning $Mn^{2+}$ emission from its usual 2.12 eV toward lower energy end, using $Mn^{2+}$-doped ZnSe NCs, either by overgrowing a thick ZnSe outer shell or by using an organic capping agent, which is a stronger ligand. Interestingly, however, the systematic decrease in the emission energy was attributed[5] to a progressive *decrease* in the crystal field splitting of $Mn^{2+}$ d electrons because of the more symmetric lattice field around the $Mn^{2+}$ ion attained by both the ZnSe outer shell and the stronger capping ligand. This explanation is intriguing in view of the well established[20] fact that the $^4T_1-^6A_1$ transition energy for $Mn^{2+}$ d electrons *decreases* with an increase in the *ligand field*, evident in the Tanabe−Sugano diagram. Also, the ligand field around a $Mn^{2+}$ ion in bulk ZnSe is not less symmetric compared to the doped NCs with both thicker ZnSe outer shell and stronger capping ligand but still it emits at the usual ∼2.12 eV,[21] as opposed to the observed red shift for the later cases. Thus it is clear that there is no real understanding of the stray example of tunability of $Mn^{2+}$ emission in ref 5. Interestingly, most works report $Mn^{2+}$ emission invariably at ∼2.12 eV independent not only of the NC size but also of the host material, such as ZnS, ZnSe, CdS or CdSe, suggesting a very similar ligand field effect on doped $Mn^{2+}$ ions, irrespective of the host size or the nature of the ligand ions.[1−8]

Having emphasized the constancy of dopant $Mn^{2+}$ ions in most cases, we note that there are, however, stray cases reported in the literature[13,22] with distinctly different $Mn^{2+}$ emission energies. For example, ref 22 reported a much lower (1.92 eV) $Mn^{2+}$ emission energy. Whereas there is no explanation or understanding so far of such rare exceptions, it motivated us to seek a proper understanding of these issues, leading to a possible

* To whom correspondence should be addressed. E-mail: sarma@sscu.iisc.ernet.in. Also at Jawaharlal Nehru Centre for Advanced Scientific Research, Bangalore-560054, India.
† Indian Institute of Science.
‡ S. N. Bose National Centre for Basic Sciences.
§ Tata Institute of Fundamental Research.
⊥ Now at Max Planck Institute for Solid State Research, D-70569 Stuttgart, Germany.

10.1021/jp105688w 
Published on Web 10/12/2010

tunability of $Mn^{2+}$ emission from doped NCs. Our study leads to a controlled tuning of $Mn^{2+}$ d emission color from $Mn^{2+}$-doped CdS NCs, in the range of yellow to red by varying the size of the NC. Our experiments reveal that the primary reason for the variation of the emission energy is in reality, not the quantum confinement effect of the host, but changes in the relative concentration of $Mn^{2+}$ ions in the surface, subsurface, and core regions of the NC, which is systematically changed by the adopted experimental conditions to produce a different sized host. These experimental results coupled with our ab initio theoretical studies established that $Mn^{2+}$ ions residing at surface/subsurface regions, not having a tetrahedral coordination, experience a larger and significantly *distorted* ligand field compared to those residing at the core of the NC with a pure tetrahedral coordination. This gives rise to subtle changes in the electronic structure at the transition metal site, explaining the observed tuning of the emission energy with *quantitative accuracy*. Our findings suggest that the $Mn^{2+}$ emission energy can be used as a very easy and useful probe to understand the location of emitting $Mn^{2+}$ ions in NC hosts, this information being difficult to obtain by any other tool.

## Experimental Section

$Cd(CH_3COO)_2 \cdot 2H_2O$ (3.25 mmol, 0.8662 g) and $Mn(CH_3COO)_2 \cdot 4H_2O$ (0.75 mmol, 0.1838 g) were dissolved in 40 mL dimethyl sulphoxide (DMSO), followed by the addition of 0.5 mL 1-thioglycerol to this solution. The reaction mixture was heated to the desired temperature in the 55−130 °C range with constant stirring and a solution of $Na_2S$ (2 mmol, 0.1561 g) in 10 mL deionized water was added drop by drop, similar to ref 13. The reaction mixture was maintained at that fixed temperature for 12 h under argon flow and the synthesized NCs were precipitated out by using acetone. The obtained precipitate was centrifuged and washed repeatedly with methanol and acetone. To prepare $Mn^{2+}$-doped CdS/CdS core/shell NCs, additional $Cd^{2+}$ and $S^{2-}$ solutions were added to the already isolated $Mn^{2+}$-doped CdS NCs redispersed in DMSO at 55 °C.

A PerkinElmer's LS 55 Luminescent spectrometer was used for photoluminescence (PL), recorded with a time delay in the range of 0.01 to 3.00 ms, between the excitation and detection of emission. These experimental spectra were decomposed into component spectra with Gaussian distribution using least-squares error analysis.

In view of the absence of any experimental estimate, first principle structural optimization was carried out within a plane wave pseudopotential implementation of density functional theory[23,24] to determine the bondlengths between $Mn^{2+}$ ion and its anion neighbors. Spherical clusters of CdS were constructed retaining bulk-like coordination and a diameter of 2.2 nm, which is very similar to the diameter of our synthesized $Mn^{2+}$-doped CdS NCs. The unit cell containing the cluster was defined to have an intercluster separation of 10 Å, ensuring negligible interactions between clusters and the surface of the cluster was passivated, following standard processes.[25] An $Mn^{2+}$ ion was introduced to replace a $Cd^{2+}$ ion at the subsurface and core regions of the NC in separate calculations including full geometry optimization in each case. We use a cutoff energy of 280 eV. The energy eigenvalues corresponding to the $Mn^{2+}$ induced levels were determined from an analysis of the character of the wave function.

## Results and Discussion

Transmission electron microscopy (TEM) shows (Figure S1 of the Supporting Information) that the $Mn^{2+}$-doped CdS NCs synthesized at 55, and 130 °C exhibit average diameters of 2.1 and 2.8 nm with size distributions of 12 and 9%, respectively. These are corroborated by estimates from UV−vis absorption spectra (part a of Figure S2 of the Supporting Information) using the reported[26] correlation of bandgap with size in the nanometric regime, exhibiting average diameters of 1.9, 2.1, 2.3, and 2.6 nm, for NCs synthesized at 55, 70, 100, and 130 °C respectively along with size distribution ∼10% in each case. Further, diameters obtained from low-angle X-ray diffraction (XRD) (part b of Figure S2 of the Supporting Information) also support above estimates of the average diameters. Atomic absorption spectroscopy (AAS) reveals 1.9, 1.4, 1.1, and 1.0% of manganese in the final product NCs synthesized at 55, 70, 100, and 130 °C respectively for the given 25% $Mn^{2+}$-precursor concentration; this decrease in manganese concentration with an increase in reaction temperature is consistent with earlier reports.[13,27,28]

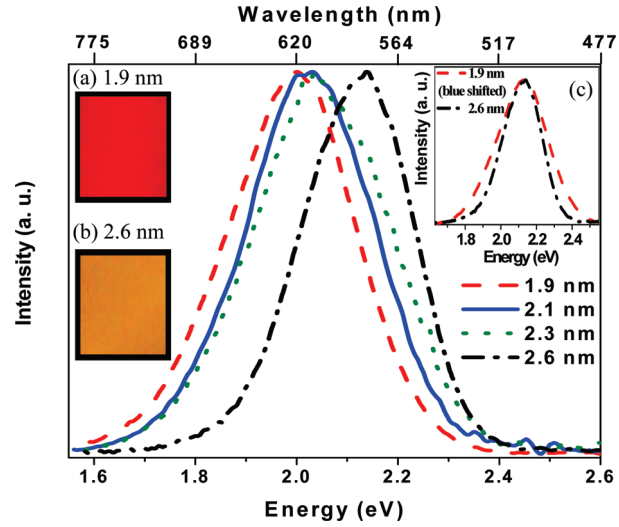


**Figure 1.** Photoluminescence spectra with a time delay of 0.05 ms between the excitation and detection of emission, for $Mn^{2+}$-doped CdS NCs with different particle sizes. Inserts a and b show steady-state emission colors for $Mn^{2+}$-doped CdS NCs with diameters of 1.9 and 2.6 nm, respectively. Insert c shows the same time delayed spectra taken from the mainframe, but after blue-shifting the spectrum for the 1.9 nm sample, such that its peak position is the same as that for the 2.6 nm sample. Each of the spectra was normalized at their corresponding maximum intensity.

A well-known difficulty of probing the intrinsic $Mn^{2+}$ emission signature obtained from a $Mn^{2+}$-doped CdS NC is the strong overlap of this emission feature with that arising from surface or defect states of the host.[13] Figure 1 shows the PL spectra with 0.05 ms delay between the excitation and detection of emission for $Mn^{2+}$-doped CdS NCs, synthesized at different reaction temperatures. These time-delayed spectra correspond entirely to $Mn^{2+}$ d emission having PL lifetime on the order of milliseconds and do not have any contribution from surface state emissions of the host that have a PL lifetime on the order of nanoseconds,[13,29] allowing us to probe only the $Mn^{2+}$ emission. PL excitation spectra (Figure S3 of the Supporting Information) with 0.05 ms delay between the excitation and detection for samples synthesized at 55 and 130 °C exhibit lowest energy peaks at ∼3.3 and 3.1 eV corresponding to bandgaps of respective CdS NC hosts. This shows that the time-delayed emission is arising only from $Mn^{2+}$ centers in the CdS NC host, via host to dopant energy transfer. A systematic and substantial blue-shift in the $Mn^{2+}$ d emission peak is observed in Figure 1 over a range of ∼0.14 eV (equivalent to ∼40 nm), changing

the $Mn^{2+}$ emission color from red to yellow, with an increase in the nanoparticle diameter from 1.9 to 2.6 nm, induced by changing the reaction temperature from 55 to 130 °C. Inserts a and b of Figure 1 show the photographs of time-integrated steady-state emission from two samples with average diameters of 1.9 and 2.6 nm, synthesized at 55 and 130 °C respectively, with the emission color of the sample being essentially determined by the dopant emission in all these cases.

To understand the origin of this systematic shift in $Mn^{2+}$ dopant emission (Figure 1), we investigate not only the emission peak position but also the emission spectral shape. For a better comparison, the time-delayed spectrum for the 1.9 nm sample was blue-shifted, such that its peak position is the same as that for the 2.6 nm sample; the resulting plots are shown in insert c of Figure 1. Evidently, the fwhm exhibited by the spectrum of 1.9 nm sample is substantially larger than that of the 2.6 nm sample. Similarly, systematic changes are also observed for samples with intermediate sizes, showing a monotonic increase in fwhm with decreasing NC size.

While we are relating changes in the emission spectra with changing size of the NC synthesized at different temperatures, we have already shown that there is also a simultaneous change in the extent of doping for a fixed precursor concentration, though retaining the same zinc-blende structure for all samples, as shown by the selected area electron diffraction patterns for two extreme samples in Figure S4 of the Supporting Information. Thus, it becomes necessary to understand independently the possible influences of particle size and extent of doping on $Mn^{2+}$ d emission energy. We investigate this issue by doping different extent of manganese in to a fixed sized CdS NC. Part a of Figure 2 shows that the $Mn^{2+}$ d emission energy is not significantly influenced by the extent of doping. Though we observe a small red shift (~0.01 eV or ~5 nm) in emission spectra with an increase in manganese concentration from 0.1 to 1.9% for samples synthesized at a fixed reaction temperature of 55 °C similar to previous reports[30,31] this is an order of magnitude smaller compared to the huge shift of ~0.14 eV (~40 nm) observed in Figure 1. Therefore, experimentally observed huge shifts in the $Mn^{2+}$ emission energy cannot be explained based on a change in manganese concentration. In fact, $Mn^{2+}$ d emission for both 0.1% and 1.9% doped samples synthesized at 55 °C is significantly red-shifted compared to that of 1% doped sample synthesized at 130 °C. Therefore, it is clear that the tunability of the $Mn^{2+}$ emission energy is associated with the changing size of the NCs rather than being due to the changing concentration of $Mn^{2+}$ ions. We, however, note that the strong dependence of the $Mn^{2+}$ emission energy on size is somewhat counterintuitive, both due to the atomic nature of the $Mn^{2+}$ levels involved in the transition and the relatively narrow range of diameter variation (1.9−2.6 nm) in these samples.

A careful observation shows that none of the spectra shown in Figure 1 is symmetric in shape, exhibiting an extra spread toward the lower energy side, whereas the emission from a single source is expected to be symmetric in the energy axis. This spectral asymmetry suggests the possibility of more than one kind of $Mn^{2+}$ ions, contributing to the observed $Mn^{2+}$ emission spectrum. Additionally, time-delayed PL spectra of these samples, for example, the 1.9% $Mn^{2+}$-doped 1.9 nm CdS NCs, exhibit a variation in the emission energy when recorded at different delay times between the excitation and detection of emission, as evident from part b of Figure 2. We find that the maximum in the emission spectrum varies systematically from 2.00 eV (620 nm) for 0.01 ms time delay to 2.06 eV (602 nm) for 3.00 ms time delay, resulting a total shift of 18 nm. This

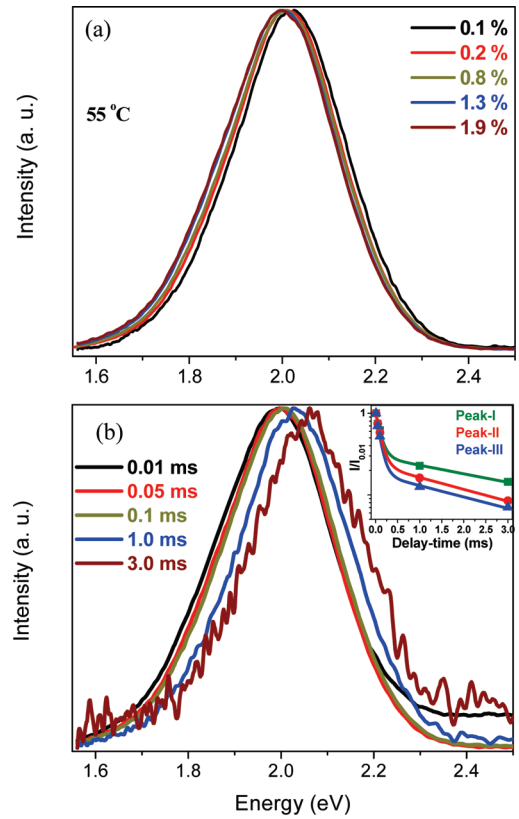


**Figure 2.** (a) Photoluminescence spectra with a time delay of 0.05 ms between the excitation and detection of emission for $Mn^{2+}$-doped CdS NCs synthesized at 55 °C but with different $Mn^{2+}$ concentrations. (b) Photoluminescence spectra with different delay times between the excitation and detection of emission, for 1.9% $Mn^{2+}$-doped 1.9 nm CdS nanocrystals synthesized at 55 °C. Each of the spectra was normalized at their corresponding maximum intensity. The insert shows the variation of PL intensity, $I/I_{0.01}$ ($I_{0.01}$ is the intensity at 0.01 ms delay) for energies corresponding to positions of peaks I, II and III, with delay time.

observation is consistent with the assumption of more than one kind of $Mn^{2+}$ ions contributing to the overall emission spectrum, because the PL lifetime for the d−d transition arising from different kinds of $Mn^{2+}$ species can be somewhat different. On the basis of these observations, we have decomposed each of the time-delayed PL spectra in terms of symmetric, component spectra using least-squares error analysis. In every case, we found it both necessary and sufficient to involve three distinct components to provide a realistic description of the experimental spectra; using only two components lead to poor and inconsistent fits, whereas using four or more components often led to unphysical negative intensity solutions. Representative results for 1.9 and 2.6 nm samples are shown in parts a and b of Figure 3, respectively. In both panels, the solid line overlapping the experimental spectrum (open circles) is the overall fit, suggesting a very realistic description of the experimental data in terms of three distinct components in the emission; broken lines in each panel correspond to component spectra arising from different kinds of $Mn^{2+}$ ions contributing to the overall emission spectrum. These three component spectra, labeled as peaks I, II, and III in the figure, appear at 2.14 ± 0.006, 2.01 ± 0.006, and 1.86 ± 0.005 eV, with fwhm values ~0.18 ± 0.005, 0.19 ± 0.005, and 0.22 ± 0.008 eV, respectively. It is important to note the extremely small error bars on these peak positions and peak widths, as determined by the spectral fitting analysis of fourteen distinct, experimentally recorded PL spectra in the present work. This proves a remarkable consistency between

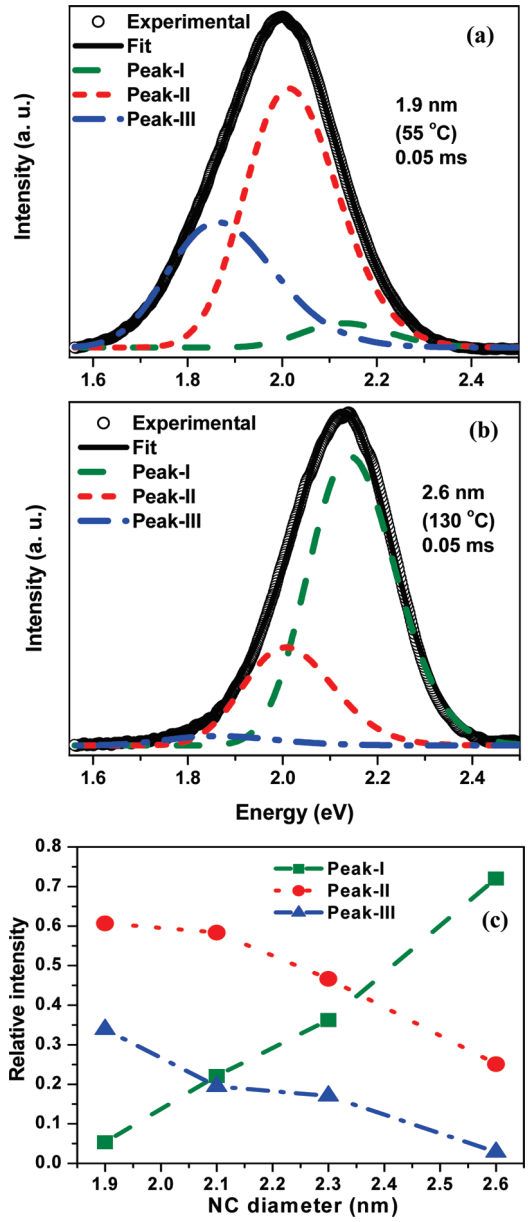


**Figure 3.** PL spectra with a time delay of 0.05 ms between the excitation and detection of emission, for $Mn^{2+}$-doped CdS NCs of (a) 1.9 nm (synthesized at 55 °C) and (b) 2.6 nm (synthesized at 130 °C) diameter, were decomposed using least-squares error analysis. In both these cases, open circles represent the experimental spectra and the overlapping solid lines are corresponding overall fits. Dashed olive lines, short-dashed red lines and dash-dot blue lines represent the component spectra labeled as peaks I, II, and III, respectively. (c) Relative intensities of peaks I, II, and III as a function of NC size is shown by the olive squares, red circles, and blue triangles, respectively; broken lines connecting these symbols are just guides to eye.

all spectral decompositions performed, thereby establishing an overall reliability of the fitting procedure and physical origins of these three components derived. To add further confidence to our spectral fitting leading to the three component spectra (peaks I, II, and III), preliminary results on spatially resolved PL measurements are shown in Figure S5 of the Supporting Information. These spectra obtained from different locations in the sample volume in a highly diluted dispersion, though noisy in our preliminary study, indeed provide evidence of components that we had earlier discerned by spectral fitting. It is to be noted that PL spectra (part b of Figure 2) with different delay times for 1.9% $Mn^{2+}$-doped 1.9 nm CdS NCs synthesized at 55 °C, could also be fitted equally well following the same procedures used in Figure 3. The insert of part b of Figure 2 shows the time-dependent PL intensity, $I/I_{0.01}$, plots where $I_{0.01}$ is the intensity for 0.01 ms delay at emission energies corresponding to peak positions of components I, II, and III. The corresponding experimental PL spectra with different delay times are shown in Figure S6 of the Supporting Information in an absolute intensity scale. The insert of part b of Figure 2 shows that different components have substantially different lifetimes in the order of peak I > peak II > peak III. The distinctly different lifetimes at these different emission energies indicate once again the existence of different Mn species in the sample.

Part c of Figure 3 shows the variation of relative intensities of peaks I, II, and III as a function of the NC size. Clearly, the relative intensity of peak I increases systematically with an increase in the NC size. In contrast, relative intensities of peaks II and III decrease with an increase in the particle size. It is this variation in the relative intensities of these three component spectra that explain the variation in peak positions and fwhm of experimental spectra (Figure 1) with the NC size. For example, the emission spectrum for the 1.9 nm sample has major (61%) contribution from peak II (2.01 eV) and thus exhibit a maximum at 2.00 eV, whereas that for the 2.6 nm sample has 72% contribution from peak I (2.14 eV), exhibiting a maximum at 2.14 eV. Peak I with a maximum at ~2.14 eV matches well with the observed emission maximum in $Mn^{2+}$-doped bulk samples[32] and therefore is assigned to $Mn^{2+}$ ions situated at the $Cd^{2+}$ substitutional site in the interior of the NC in present samples. This interpretation is further supported by the fact that an increase in the particle diameter from 1.9 to 2.6 nm leads to a substantial increase in the relative contribution of peak I to the overall spectrum (part c of Figure 3). Obviously, the larger particle has a smaller surface to bulk ratio, leading to a higher probability of $Mn^{2+}$ incorporation in the interior of the NC than on its surface. With peak I appearing at 2.14 eV assigned to $Mn^{2+}$ ions at the interior of the NC, it is natural to attribute lower energy emissions at 2.01 and 1.86 eV (peaks II and III) from different kinds of $Mn^{2+}$ ions situated near the surface/subsurface regions of the NC. It is clear from the plots that there is a rapid increase in the combined intensities of surface related $Mn^{2+}$ emissions (peaks II and III together) with a decreasing particle size. This observation is consistent with the fact that the total volume attributable to the surface layer compared to the volume associated with the core of the particle increases rapidly with a decreasing particle size. This alone may quantitatively explain the changes in the surface related emissions (peaks II and III) compared to that from the core-doped Mn (peak I) as a function of the particle size (part c of Figure 3) if we assume a homogeneous distribution of $Mn^{2+}$ ions throughout the nanoparticles along with a surface thickness of about 1.4 times the unit cell parameter. However, it is quite plausible that the $Mn^{2+}$ ions are inhomogeneously distributed within the nanoparticles with smaller nanoparticles having a higher proportion of surface Mn concentration as compared to that in larger nanoparticles; this is supported by our earlier observation (ref 13) that smaller NCs have a higher tendency to drive $Mn^{2+}$ ions out toward the surface compared to larger particles for a given concentration of doping. We believe that both these effects, namely a rapid increase in the relative contribution from the surface layer with decreasing particle size and a preferential populating of the surface layer with doped $Mn^{2+}$ ions in smaller particles, together are responsible for the observed trend shown in part c of Figure 3, exhibiting a rapid

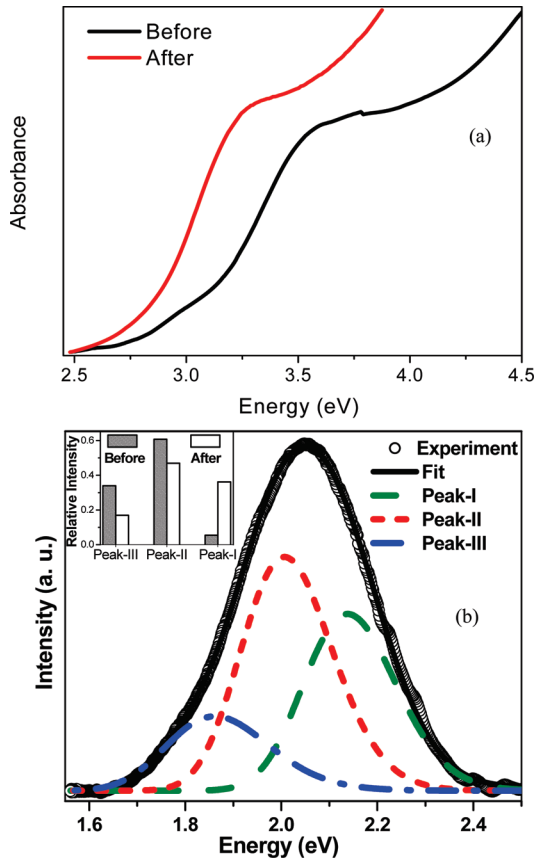


**Figure 4.** (a) UV−vis absorption spectra for samples, before (1.9% $Mn^{2+}$-doped CdS NCs) and after (1.9% $Mn^{2+}$-doped CdS/CdS core/shell NCs) shell formation. Each of the spectra was normalized at their corresponding maximum absorbance. (b) Decomposition of the PL spectrum with a time delay of 0.05 ms between the excitation and detection of emission, for 1.9% $Mn^{2+}$-doped CdS/CdS core/shell NCs. Open circle represents the experimental spectrum, overlapping solid line is the overall fit and the broken lines represent component spectra labeled as peaks I, II, and III. Insert compares the relative intensities of peaks I, II, and III contributing to the overall spectra for the samples, before (1.9% $Mn^{2+}$-doped CdS NCs) and after (1.9% $Mn^{2+}$-doped CdS/CdS core/shell NCs) shell formation.

increase in the relative emission intensity of surface related $Mn^{2+}$ ions with a decreasing particle size.

To probe and establish the nature and origin of these three component spectra, we have grown a CdS shell on top of the already prepared 1.9% $Mn^{2+}$-doped 1.9 nm CdS core NCs, where the temperature of the core formation and shell growth were kept fixed at 55 °C. UV−vis absorption spectrum of the 1.9% $Mn^{2+}$-doped CdS/CdS core/shell NCs is significantly red-shifted compared to that of the core NCs as shown in part a of Figure 4. The bandgap of the core/shell sample is found to be 3.05 eV, corresponding[26] to 2.5 nm sized CdS NCs, suggesting the formation of about a monolayer of CdS shell on top of the 1.9 nm sized $Mn^{2+}$-doped CdS core. In the present context, it is most important to note that the $Mn^{2+}$ d emission of the sample is significantly blue-shifted with a maximum at 2.05 eV (605 nm) after the shell formation (open circles in part b of Figure 4), compared to that (2.00 eV or 620 nm, as shown in part a of Figure 3) before the shell formation. The spectrum after the shell formation was decomposed in the same way as described for those in Figure 3 and the component spectra along with the overall fit are presented in part b of Figure 4. Variations in relative intensities of peaks I, II, and III obtained from part a of Figure 3 and Figure 4, for the samples before and after the

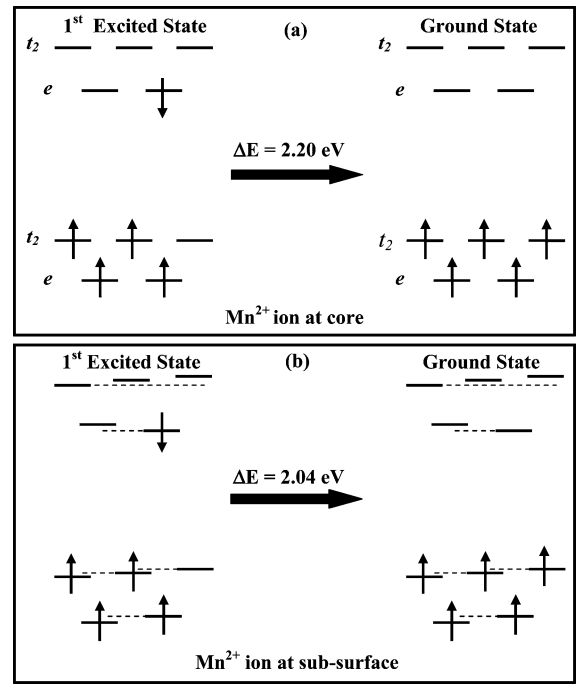


**Figure 5.** Schematic energy-level diagrams showing the crystal field splitting of d levels for $Mn^{2+}$ ions at the (a) core and (b) subsurface of a CdS cluster. Dashed lines in part b of Figure 4 are just a guide to eye showing the lifting of degeneracy of $e$ and $t_2$ levels.

shell formation respectively, are shown by bar diagrams in the insert of part b of Figure 4. Clearly, relative intensity of peak I increases by ∼7 times after the shell formation, whereas relative intensities of both peaks II and III decrease substantially after the shell growth. To crosscheck that the blue shift in $Mn^{2+}$ emission is indeed due to the shell formation and not influenced by the additional heating at 55 °C during the shell formation, we heated the dispersion of 1.9% $Mn^{2+}$-doped 1.9 nm CdS core NCs in DMSO at 55 °C for the same extra duration (∼3 h); however, we did not observe any change in absorption and emission spectra. These results strongly support our previous assignments of peak I arising from a core $Mn^{2+}$ substitution and peaks II and III from dopants near the surface regions. These results also show that the difference in reaction temperature employed for the synthesis of nanocrystals with different sizes is not crucial in determining the energy of $Mn^{2+}$ emission because both the core and core/shell particles prepared at the same temperature (55 °C) exhibit very different $Mn^{2+}$ emission energies.

To establish above interpretations conclusively, we have carried out state-of-the-art ab initio electronic structure calculations with full geometry optimization to determine d−d transition energies for $Mn^{2+}$ ions residing at different locations in such an NC. The energy minimization leads to all four $Mn^{2+}$−$S^{2-}$ bondlengths for the case of core-doping to be 2.43 Å with a perfect tetrahedral symmetry. In contrast, for the subsurface $Mn^{2+}$ ion, $MnS_4$ tetrahedra is found to be distorted with $Mn^{2+}$−$S^{2-}$ bondlengths being 2.41, 2.41, 2.42, and 2.43 Å. To arrive at energy-level diagrams for $Mn^{2+}$ 3d levels in each case, eigenvectors of different energy eigenvalues from these self-consistent electronic structure calculations were analyzed for their symmetry, the dominant atom type and angular momentum character; these analysis yield energy-level diagrams as shown in parts a and b of Figure 5 for 3d levels of $Mn^{2+}$ ions at the core and subsurface of the CdS cluster, respectively. In the case of the $Mn^{2+}$ ion at the core, the doubly

degenerate eigenvalues in the up-spin channel with dominantly $Mn^{2+}$ character are identified as levels with *e* symmetry, whereas the triply degenerate levels with dominantly $Mn^{2+}$ character are identified as $Mn^{2+}$ 3d levels with $t_2$ symmetry, as shown in part a of Figure 5. The distortion in the $MnS_4$ tetrahedron near the surface region lifts the degeneracy of *e* and $t_2$ levels, as shown in part b of Figure 5; this is further contributed by the presence of the terminating surface in the close vicinity on only one side of the $MnS_4$ unit, making the electronic potential even more asymmetric with respect to the centrally located $Mn^{2+}$ ion.

$Mn^{2+}$ ion with five unpaired electrons defines the ground state as shown in the right-hand side of part a of Figure 5, where all the up-spin *e* and $t_2$ states are occupied, giving rise to a total spin multiplicity of 6. However, for the first excited state, one of the up-spin $t_2$ electron of the ground state is replaced with a down-spin *e* electron, leading to a total spin multiplicity of 4, as shown in the left-hand side of part a of Figure 5. When we express electron−electron interaction strengths within the Mn d orbitals in terms of intra-atomic direct (*U*) and exchange ($J_H$, also known as the Hund's coupling strength) interaction strengths, the splitting between the up and down-spin energy levels in part a of Figure 5 is given by $4J_H$. The *d*−*d* transition energy between the first excited state to the ground state in part a of Figure 5 is calculated to be $(4J_H - 0.60)$ eV on the basis of the energetics of the ligand-field level diagrams obtained from our ab initio calculations. Carrying out the same analysis for the near-surface distorted tetrahedral case shown in part b of Figure 5, we obtain the transition energy between first excited state and the ground state to be $(4J_H - 0.76)$ eV. Thus, the difference between the $Mn^{2+}$ d−d transition energies calculated for $Mn^{2+}$ ion in the core and subsurface ($\{4J_H - 0.60\} - \{4J_H - 0.76\} = 0.16$ eV) is 0.16 eV and is independent of $J_H$. This value agrees well with the experimentally obtained difference between peak I and peak II (0.13 eV), thereby reconfirming the fact that peak II originates from $Mn^{2+}$ ions residing in the subsurface of these NCs with a distorted tetrahedral environment around the $Mn^{2+}$ ion. In view of these results, we believe that the third emission component, peak III (1.86 eV), is from $Mn^{2+}$ ions at the surface region with a 1-thioglycerol capping, because this situation would provide an even more strongly distorted ligand field and a consequent lifting of the d level degeneracies to a greater extent, this lifting of the degeneracy rather than the absolute strength of the ligand field being the driving force for the observed red-shift from peak I, to peak II, to peak III. It is to be noted here that an ab initio calculation with such a large sized cluster together with all flexibilities of capping agents including geometry optimization is way beyond the computational infrastructure available at present.

In passing, we note that a perfect agreement between the calculated position of peak I $(4J_H - 0.60)$ with the experimental value of 2.14 eV can be obtained by setting $J_H = 0.685$ eV; this choice of $J_H$ also leads to a good estimate $(4J_H - 0.76 = 1.98$ eV) of peak II position when compared with the experimentally obtained value of 2.01 eV. Earlier analysis[33] of ab initio band structure results for Mn oxides estimated $J_H$ to be ~0.8 eV. We expect a lower value of $J_H$ for sulphides that form compounds with wider band widths than corresponding oxides, as screening effects[34,35] are more efficient in such cases, lowering $J_H$ somewhat, indicating the required value of $J_H$ for a good agreement between experimental PL positions and calculated ones to be a reasonable one based on the past literature.

## Conclusions

The color of $Mn^{2+}$ d emission from $Mn^{2+}$-doped CdS NCs could be tuned systematically by ~0.14 eV (40 nm) in the red-yellow region by controlling the particle diameter between 1.9 and 2.6 nm. $Mn^{2+}$ ions residing at the interior, subsurface, and surface of the NC exhibit emissions at 2.14, 2.01, and 1.86 eV respectively due to the lifting of degeneracies of the d levels arising from local distortion in the $MnS_4$ tetrahedra and a subtle consequent change in the ligand field. Each of these emissions from three distinct dopant sites is insensitive to the NC size but a decrease in NC size results into an increase in surface to bulk ratio, thereby increasing the relative contributions of surface and subsurface $Mn^{2+}$ ions to the overall emission spectra, leading to a red shift in the overall $Mn^{2+}$ emission. This understanding, while allowing us to tune the $Mn^{2+}$ d emission from the same system of $Mn^{2+}$-doped CdS NCs, additionally provides an easy and unique tool to obtain the location of an emitting $Mn^{2+}$ ion inside the NC from the peak position of the emission spectrum.

**Acknowledgment.** Authors acknowledge Department of Science and Technology as well as Board of Research in Nuclear Sciences, Government of India, for funding the project. DDS acknowledges J. C. Bose National Fellowship.

**Supporting Information Available:** Details of experimental section, TEM image, UV−vis absorption, low-angle XRD patterns, and SAED patterns of $Mn^{2+}$-doped CdS NCs with different sizes are given. Spatially resolved PL spectra of isolated NCs for 1.9 nm $Mn^{2+}$-doped CdS NCs. This material is available free of charge via the Internet at http://pubs.acs.org.

## References and Notes

(1) Bhargava, R. N.; Gallagher, D.; Hong, X.; Nurmikko, A. *Phys. Rev. Lett.* **1994**, *72*, 416–419.
(2) Erwin, S. C.; Zu, L.; Haftel, M. I.; Efros, A. L.; Kennedy, T. A.; Norris, D. J. *Nature* **2005**, *436*, 9–94.
(3) Yang, Y.; Chen, O.; Angerhofer, A.; Cao, C. J. *J. Am. Chem. Soc.* **2006**, *128*, 12428–12429.
(4) Nag, A.; Sarma, D. D. *J. Phys. Chem. C* **2007**, *111*, 13641–13644.
(5) Pradhan, N.; Peng, X. *J. Am. Chem. Soc.* **2007**, *129*, 3339–3347.
(6) Nag, A.; Chakraborty, S.; Sarma, D. D. *J. Am. Chem. Soc.* **2008**, *130*, 10605–10611.
(7) Beaulac, R.; Archer, P. I.; Liu, X.; Lee, S.; Salley, G. M.; Dobrowolska, M.; Furdyna, J. K.; Gamelin, D. R. *Nano Lett.* **2008**, *8*, 1197–1201.
(8) Nag, A.; Sapra, S.; Gupta, S. S.; Prakash, A.; Ghangrekar, A.; Periasamy, N.; Sarma, D. *D Bull. Mater. Sci.* **2008**, *31*, 561.
(9) Murray, C. B.; Norris, D. J.; Bawendi, M. G. *J. Am. Chem. Soc.* **1993**, *115*, 8706–8715.
(10) Burda, C.; Chen, X.; Narayanan, R.; El-Sayed, M. A. *Chem. Rev.* **2005**, *105*, 1025–1102.
(11) Kongkanand, A.; Tvrdy, K.; Takechi, K.; Kuno, M.; Kamat, P. V. *J. Am. Chem. Soc.* **2008**, *130*, 4007–4015.
(12) Nag, A.; Kumar, A.; Kiran, P. P.; Chakraborty, S.; Kumar, G. R.; Sarma, D. D. *J. Phys. Chem. C* **2008**, *112*, 8229–8233.
(13) Nag, A.; Sapra, S.; Nagamani, C.; Sharma, A.; Pradhan, N.; Bhat, S. V.; Sarma, D. D. *Chem. Mater.* **2007**, *19*, 3252–3259.
(14) Yang, H.; Holloway, P. H. *J. Phys. Chem. B* **2003**, *107*, 9705–9710.
(15) Yang, H.; Holloway, P. H.; Ratna, B. B. *J. Appl. Phys.* **2003**, *93*, 586.
(16) Pradhan, N.; Battaglia, D. M.; Liu, Y.; Peng, X. *Nano Lett.* **2007**, *7*, 312–317.
(17) Thakar, R.; Chen, Y.; Snee, P. T. *Nano Lett.* **2007**, *7*, 3429–3432.
(18) Viswanatha, R.; Chakraborty, S.; Basu, S.; Sarma, D. D. *J. Phys. Chem. B* **2006**, *110*, 22310–22312.
(19) Xie, R.; Peng, X. *J. Am. Chem. Soc.* **2009**, *131*, 10645–10651.
(20) Beaulac, R.; Archer, P. I.; Gamelin, D. R. *J. Solid State Chem.* **2008**, *7*, 1582.
(21) MacKay, J. F.; Becker, W. M.; Spaek, J.; Debska, U. *Phys. Rev. B* **1990**, *42*, 1743–1749.
(22) Tanaka, M.; Qi, J.; Masumoto, Y. *J. Cryst. Growth* **2000**, *214/215*, 410–414.
(23) Kresse, G.; Furthmüller, J. *Phys. Rev. B* **1996**, *54*, 11169–11186.
(24) Kresse, G.; Furthmüller, J. *Comput. Mater. Sci.* **1996**, *6*, 15–50.
(25) Cherian, R.; Mahadevan, P. *Phys. Rev. B* **2007**, *76*, 075205.

(26) Sapra, S.; Sarma, D. D. *Phys. Rev. B* **2004**, *69*, 125304.

(27) Levy, L.; Feltin, N.; Ingert, D.; Pileni, M. P. *J. Phys. Chem. B* **1997**, *101*, 9153–9160.

(28) Chan, T.-L.; Zayak, A. T.; Dalpian, G. M.; Chelikowsky, J. R. *Phys. Rev. Lett.* **2009**, *102*, 025901.

(29) Sapra, S.; Prakash, A.; Ghangrekar, A.; Periasamy, N.; Sarma, D. D. *J. Phys. Chem. B* **2005**, *109*, 1663–1668.

(30) Suyver, J. F.; Wuister, S. F.; Kelly, J. J.; Meijerink, A. *Phys. Chem. Chem. Phys.* **2000**, *2*, 5445.

(31) Chen, H.-Y.; Chen, T.-Y.; Son, D. H. *J. Phys. Chem. C* **2010**, *114*, 4418.

(32) Goede, O.; Heimbrodt, W. *Phys. Status Solidi B* **1988**, *146*, 11–62.

(33) Mahadevan, P.; Shanthi, N.; Sarma, D. D. *J. Phys.: Condens. Matter* **1997**, *9*, 3129.

(34) Sarma, D. D.; Kamath, P. V. *Phys. Rev. B* **1987**, *36*, 7402–7406.

(35) Bandyopadhyay, T.; Sarma, D. D. *Phys. Rev. B* **1989**, *39*, 3517–3521.

JP105688W